Suppression of aliasing artifacts on 3D land data via Constrained Least-Squares Migration

Alejandro Cabrales-Vargas, Pemex Exploración y Producción; University of Oklahoma*
Kurt Marfurt and Bo Zhang, University of Oklahoma

Summary

Kirchhoff migration has the ability of handling irregularly acquired seismic data without previous trace interpolation, in contrast with wave-equation continuation and finite-difference migration. However, aliasing noise as acquisition footprint frequently affects the migrated gathers making difficult or even impossible the application of AVO and elastic inversion. In addition, irregular acquisition affects the completeness of the data resulting in the missing traces, which negatively impacts velocity analysis required by depth migration. Constrained least-squares migration allows us both to reduce the aliasing related artifacts and the prediction of the missing traces. CLSM is implemented by iteratively minimizing the difference between the input data and the modeled data from the proposed reflectivity, in this case the migrated data. Modeling is implemented through demigration, with the minimization implemented through the conjugate gradient method. Using a penalty function we restrict the reconstruction of the data to geological constraints (e.g., smooth variation in the offset domain). A by-product is the prediction of missing traces in irregularly acquired datasets. The main disadvantage of CLSM is the considerable increase in computing time.

Introduction

When considering migration of irregularly sampled 3D data, Kirchhoff migration is the often the best choice, being computationally efficient and avoiding trace interpolation of the input data. Nevertheless, Kirchhoff migration exhibits important flaws. Operator and data aliasing constitute the main drawback of the Kirchhoff algorithm. In the shallow parts of the final volume these artifacts results in acquisition footprint. This leaked noise and migration artifacts seriously interfere with the ability of the interpreter to identify geological features of interest.

The inaccuracy of the migration operator applied to sparse surface measurements to approximate the inverse of the forward modeling operator is a function of the acquisition geometry (Nemeth, 1996). Irregularly sampled data make velocity analysis ambiguous and prone to errors. Data aliasing and acquisition footprint are other important consequences of these irregularities. Least-squares migration has been investigated by Nemeth (1996), Nemeth et al. (1999), Schuster (1997), and many others, with the objective of attenuating acquisition footprint and data aliasing while minimizing the loss of geological signal that can occur using more conventional filtering methods. The cost of the computation of least-squares migration is directly proportional to the number of iterations. For this reason, significant effort has addressed preconditioning the data and/or the matrices to reduce the need to invert them.

Constrained Least-Squares Migration (CLSM) consists of minimizing the residual error (in a least-squares sense) between the data and the remodeled data obtained by demigrating the filtered (or otherwise constrained) migrated gathers, which constitute our approximation to the Earth's reflectivity. After the computation of the residual error the model (migrated gathers) is updated and the process is repeated until the minimum criterion is met or the desired number of iterations is reached.

The advantages of CLSM when compared with conventional prestack time Kirchhoff migration are better estimation of the reflectivity of the subsurface in a least-squares sense (Duquet et al., 2000), reduction of aliasing artifacts, acquisition footprint, ground-roll and other coherent noise, and the improvement of the signal-to-noise ratio of common-reflection point gathers (a vital factor in prestack analysis such as AVO and elastic inversion).

Constrained Least-Squares Migration theory

We can express modeling and migration in matrix notation as follows:

$$\mathbf{d} = \mathbf{G}\mathbf{m}, \quad \text{and} \tag{1}$$

$$\mathbf{m}' = \mathbf{G}^{\mathrm{T}}\mathbf{d}, \tag{2}$$

where **G** constitutes the forward modeling operator, **m** is the regularly sampled model (Chemingui and Biondi, 2002) that represent the Earth's reflectivity, $\mathbf{G}^{\mathrm{T}}$ is the adjoint operator and **m'** is the estimation of the true Earth's reflectivity **m** using such an operator. We use Kirchhoff demigration to represent the forward modeling operator and Kirchhoff migration to represent the adjoint operator.

Substituting equation 1 into equation 2 we obtain

$$\mathbf{m}' = \mathbf{G}^{\mathrm{T}}\mathbf{G}\mathbf{m}, \tag{3}$$

From this relation we observe that our estimated reflectivity relates to the true Earth's reflectivity through the operator $\mathbf{G}^{\mathrm{T}}\mathbf{G}$. Note that if our migration operator better approximates the inverse of the modeling process, the square matrix $\mathbf{G}^{\mathrm{T}}\mathbf{G}$ tends to the identity matrix, **I**, and the model vector **m'** tends to **m**. Nemeth (1996) observes that the elements of the matrix $\mathbf{G}^{\mathrm{T}}\mathbf{G}$ depend on the geometrical arrangement of the sources and receivers, giving rise to acquisition footprint. In the case of a dense acquisition geometry, the off-diagonal terms of the operator $\mathbf{G}^T\mathbf{G}$ become negligible such that it becomes a diagonal matrix. In contrast, irregular and sparse acquisition geometry imply that the matrix $\mathbf{G}^T\mathbf{G}$ departs from such an ideal operator.

For reasons of cost and limitations of equipment, 3D seismic data is rarely, if ever acquired uniformly in all five dimensions (Ronen and Liner, 2000). For this reason 3D seismic data frequently exhibit gaps that generate aliasing artifacts in the migrated images and limit the accuracy of the velocity analysis (Duquet et al., 2000). Additionally, the adjoint operator of migration can fail to represent every recorded event. However, the demigration operator based on our migration code ensures that only those events properly handled by the migration algorithm are modeled (Duquet et al., 2000).

Methodology

We illustrate the application of CLSM on 2D and 3D data. In the first case we use the anisotropic version of the Marmousi dataset (Alkalifah, 1997) after decimation. We compare representative common reflection point gathers, the stacked sections and the predicted data using conventional migration, unconstrained and constrained least-squares migration. In the second case we compare the migrated volumes and common reflection point gathers of the 3D Dickman dataset from West Kansas after conventional migration and constrained least-squares migration.

Numerical Results: Marmousi 2D synthetic dataset

The Marmousi dataset corresponds to the anisotropic version generated by Alkhalifah (1997). The data consist of 232 shots and 136 traces per shot, both spaced 25 m apart, for a total of 31552 traces with time sampling of 4 ms and 3 s of time recording. The velocity and anisotropy models consist of 240 vertical samples and 737 horizontal samples, with spacing of 12.5 m both dimensions.

Figure 1 shows a detail of the shot gathers. Figure 2 shows the same shot gathers after randomly killing two thirds of the traces, which were not included in the calculations. Figures 3-5 show the predicted data after conventional migration, unconstrained and constrained LSM, respectively, after five iterations. Both conventional migration and unconstrained LSM predict the data without adequately predicting the gaps and suffering from some additional background noise. Unconstrained LSM corrects the amplitudes to the order of magnitude of the data. Constrained LSM greatly improves the predicted data by attenuating the background noise and better predicting the missing traces. Note that in all the cases, the direct waves, which are particularly conspicuous at the shallow part in the original data, are not predicted by Kirchhoff demigration.

Figure 6 shows the common reflection point gather at x = 3750 m. Conventional migration and unconstrained LSM sections look almost identical, with the aliasing artifacts affecting the flat events. Constrained LSM virtually eliminates such noise.

Finally, Figures 7-9 show the final stacked sections. They are similar in quality, with some improvements of marginal events in the LSM cases.

Numerical Results: 3D Dickman dataset

The dataset use to test 3D CLSM corresponds to the Dickman 3D survey acquired by Grand Mesa Operating Company in the area of Ness county, Kansas.

Figure 10 shows the result of applying 3D conventional Kirchhoff migration to a subset of the data. Representative vertical sections and a timeslice are plotted. The shallowest timeslice was extracted from the most positive curvature attribute calculated from the original volume. Acquisition footprint can be clearly observed in both timeslices, although it is not apparent in the vertical sections. The channel in the seismic timeslice is negatively affected by the footprint and its boundaries are blurred.

Figure 11 shows the result of CLSM after 3 iterations. The seismic timeslice exhibits a significant reduction of acquisition footprint, and the channel boundaries become shaper, allowing better interpretation of subtle features such as the crevasse splay shown by the black arrow. The sections show improvements in vertical resolution and event definition, as in the reflectors indicated by the yellow arrows. In contrast, the curvature timeslice shows no significant attenuation of acquisition footprint.

Figure 12 shows the result of CLSM after 6 iterations. Now the seismic timeslice looks virtually free from acquisition footprint. The channel boundaries are even sharper, with better definition and delineations of the crevasse splay (black arrow). Note in the vertical sections the further improvement of vertical resolution. Particularly, the seismic reflector indicated with the uppermost yellow arrow exhibits better definition and a less blurred appearance, whereas the lowermost ones indicate a seismic event that now can be differentiated into two reflectors. The shallow curvature timeslice now exhibits important attenuation of the acquisition footprint, compared to Figures 10 and 11.

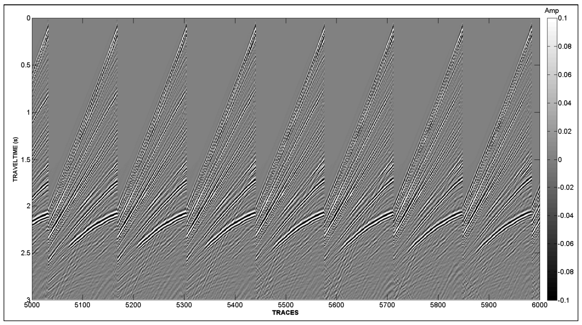

Figure 1: Representative shot gathers of the Marmousi model.

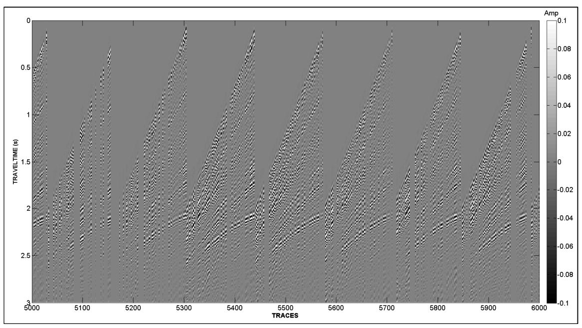

Figure 2: Shot gathers after killing two thirds of the traces.

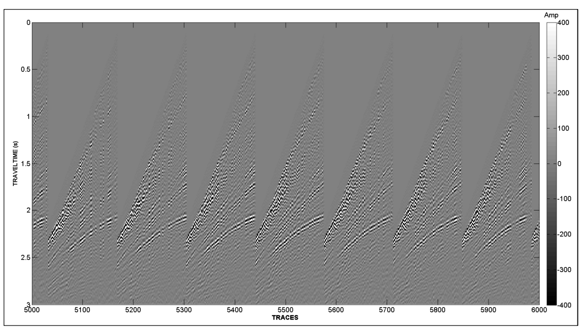

Figure 3: Predicted (modeled) shot gathers after conventional migration. Note that the gaps have not been completely interpolated.

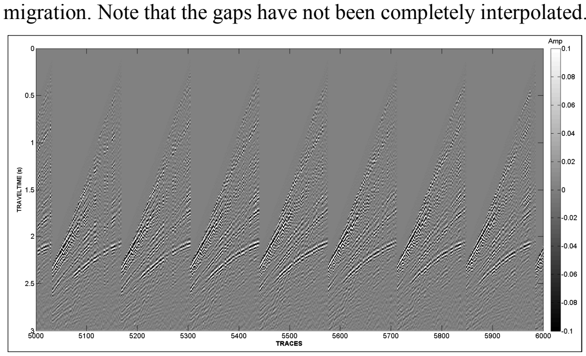

Figure 4: Predicted (modeled) shot gathers after unconstrained LSM migration. The gaps still persist.

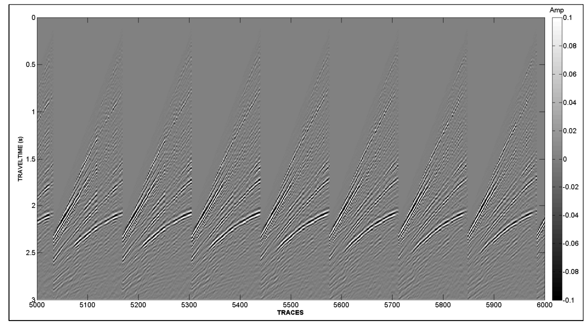

Figure 5: Predicted (modeled) shot gathers after constrained LSM migration. Now most of the gaps are healed. Compare to Figure 1.

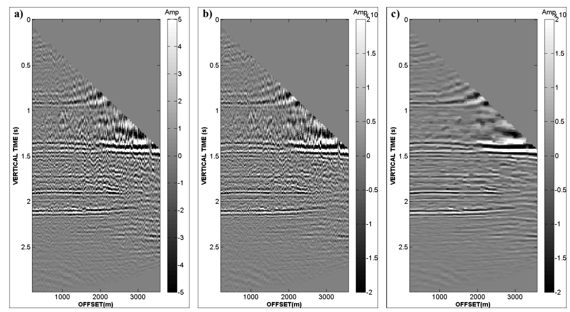

Figure 6: Common reflection point gathers at x = 3750 m for the Marmousi model from the decimated dataset using (a) conventional migration, (b) Unconstrained LSM, and (c) Constrained LSM.

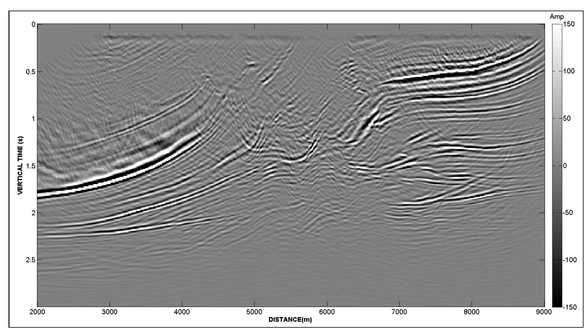

Figure 7: Stacked image over all offsets for the Marmousi model computed from the decimated dataset using conventional migration.

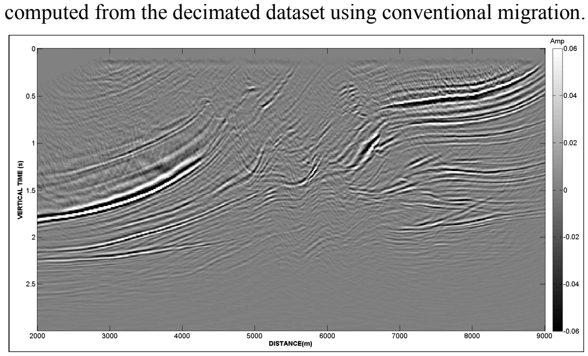

Figure 8: Stacked image over all offsets for the Marmousi model from the decimated dataset using unconstrained LSM.

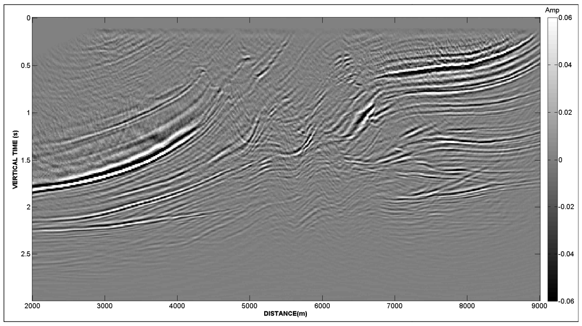

Figure 9: Stacked image over all offsets for the Marmousi model computed from the decimated dataset using constrained LSM.

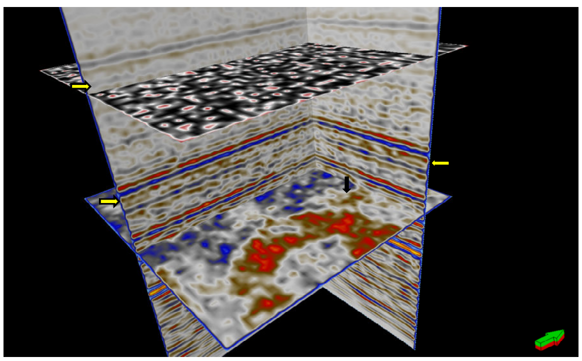

Figure 10: Dickman survey after conventional Kirchhoff migration. The seismic timeslice show a blurring appearance of the channel boundaries and features, like the crevasse splay (black arrow). It exhibits acquisition footprint, better highlighted by the curvature timeslice.

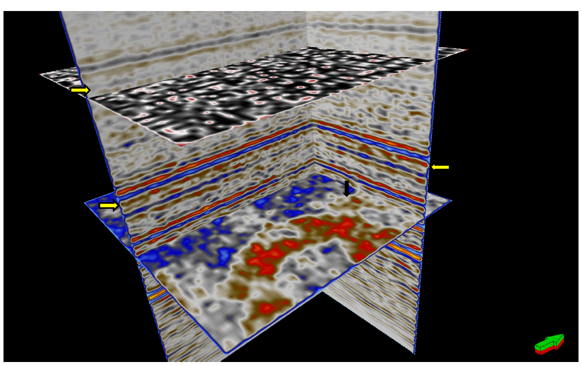

Figure 11: Dickman survey after CLSM using 3 iterations. The channel boundaries are better defined, although some acquisition footprint is still visible. Attenuation of the footprint is barely observable in the curvature timeslice.The yellow arrows show seismic reflectors that improved their definitions as a result of the increment of seismic resolution.

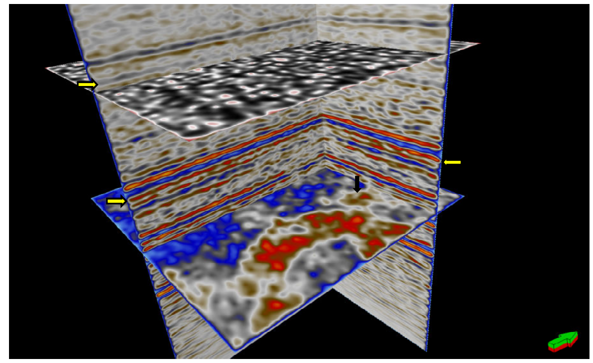

Figure 12: Dickman survey after CLSM using 6 iterations. Note the further improvement in the definition of the channel boundaries and the crevasse splay (black arrow), and the virtual absence of acquisition footprint, that now appears notably attenuated in the curvature timeslice. The seismic reflector indicated by the uppermost yellow arrow is better difined, whereas the event indicated by the lowermost yellow arrows exhibits further improvement in vertical resolution, which now allows the diferenciation of two seismic reflectors.

Conclusions

Constrained least-squares migration has the ability to restore the seismic amplitudes of both the migrated gathers and its corresponding stack, as it represents a more consistent estimation of the Earth's reflectivity than conventional migration. This fact is particularly important for prestack processing such as AVO, AVAZ, and elastic inversion, which strongly rely on the seismic amplitude. Additionally, the appropriate use of a constraint function allows the attenuation of aliasing artifacts and particularly acquisition footprint, which is due to an irregular or incomplete acquisition pattern. As a by-product there is the possibility to predict absent data traces with better signal to noise ratio, which benefits processes like detailed velocity analysis for depth migration. The main disadvantage of the method is the increase in computing time of at least twice the time of conventional migration every iteration.

We use the anisotropic Marmousi dataset to test the ability of unconstrained and constrained LSM to handle aliasing artifacts and incomplete coverage compared to conventional migration. Corresponding predicted data are compared as well. Finally, we used a subset of the 3D Dickman dataset from West Kansas to test the ability of CLSM to attenuate acquisition footprint and deblur geologic features.